Desalination and Water Treatment
www.deswater.com

doi: 10.5004/dwt.2018.21663

102 (2018) 9–15
January

Facile surface modification of a polyamide reverse osmosis membrane using a TiO_2 sol-gel derived spray coating method to enhance the anti-fouling property

Jungchan Kim[a], Choonsoo Kim[a], Youngbin Baek[a,c], Sung Pil Hong[a], Hee Joong Kim[a], Jong-Chan Lee[a], Jeyong Yoon[a,b,*]

[a]*School of Chemical and Biological Engineering, College of Engineering, Institute of Chemical Process (ICP), Seoul National University (SNU), Gwanak-gu, Daehak-dong, Seoul 08826, Korea, Tel. +82 2 880 8927; Fax: +82 2 876 8911; email: jeyong@snu.ac.kr (J. Yoon)*
[b]*Asian Institute for Energy, Environment & Sustainability (AIEES), Seoul National University (SNU), Gwanak-gu, Daehak-dong, Seoul 08826, Korea*
[c]*Department of Chemical Engineering, The Pennsylvania State University, University Park, PA 16802, USA*

Received 27 August 2017; Accepted 28 October 2017

ABSTRACT

We reported a facile surface modification by the TiO_2 sol-gel derived spray coating method to enhance the fouling resistance of a polyamide (PA) reverse osmosis (RO) membrane. TiO_2 nanoparticles (TNPs) were prepared by the base catalyzed sol-gel method for a short span of time and deposited onto the commercial PA RO membrane by spraying. The coated TNPs, which have a role as a functional layer on the PA RO membrane, made the membrane surface more hydrophilic and more negatively charged. These modified surface properties reduced the interactive force between humic acid and the membrane surface which resulted in the enhancement of fouling resistance of the PA RO membrane without losses in membrane performances such as the permeate flux and salt rejection when the proper amounts of TiO_2 were coated on the membrane. This study suggests a facile surface modification to fabricate a fouling resistant PA RO membrane by using the TiO_2 sol-gel derived spray coating method.

Keywords: Reverse osmosis; TFC membrane; TiO2 sol-gel spray coating; Surface modification

1. Introduction

Reverse osmosis (RO) is widely used and is the fastest growing desalination process [1,2]. Currently, no less than 15,000 desalination plants have been constructed, and the RO process comprises approximately 50% of those plants [3]. In the RO process, polyamide (PA) thin-film composite (TFC) membranes are dominantly used due to their high permeability, high selectivity, wide operation temperature and pH ranges [4]. Despite these advantages, membrane fouling is considered as one of the main obstacles for the RO process [5,6]. Membrane fouling causes a decrease in the membrane performance (i.e., the permeate flux and salt rejection) due to the hindering of water transport and a subsequent concentration polarization near the membrane surface which eventually increases the operating cost [7].

The fouling characteristics of a membrane are affected by its surface property such as the hydrophilicity, morphology and surface charge [8]. In general, hydrophilic, smooth and negatively charged membranes are known to have resistance to fouling because a foulant (i.e., proteins and humic acid) naturally has a hydrophobic and negatively charged surface property [9]. Based on these understandings of the membrane fouling mechanism, development of anti-fouling

* Corresponding author.

RO membranes has been actively conducted. Hydrophilic modification of the RO membrane surface by plasma polymerization [10], graft polymerization [11] and grafting poly(ethylene glycol) (PEG) [12] all have shown enhanced fouling resistance. PEG [13] or zwitterionic film coating [14] on a RO membrane also resulted in an improved anti-fouling property by increasing the steric repulsion to foulants.

Titanium dioxide (TiO_2) has been used on RO membranes to improve fouling resistance due to its advantages such as cost-effective, eco-friendly, and photo-catalytic properties [15]. For example, TiO_2 nanoparticles were self-assembled on PA TFC RO membranes to control biofouling, and the TiO_2-coated membranes exhibited a higher anti-microbial property than that of the commercial membrane under UV light [16,17]. It was also shown that organic foulants were detached from the fouled membrane, and the reduced permeate flux was recovered after UV irradiation [18]. In previous studies, the dip coating method has been usually used due to its simplicity. However, this dip coating method has a limitation, specifically a slow coating rate, which might cause low productivity in membrane manufacturing [19–21].

This paper introduced a facile surface modification for a fouling resistant PA RO membrane using the TiO_2 sol-gel derived spray coating method. TiO_2 nanoparticles (TNPs) were prepared with the base catalyzed sol-gel method and coated onto the commercial PA RO membrane with the spray coating method. The surface properties of the TNP-coated PA RO membrane were analyzed with a scanning electron microscope, X-ray photoemission spectroscopy, attenuated total reflection Fourier-transform infrared, contact angle analyzer and zeta potential analyzer. The permeate flux, salt rejection and organic fouling property of the TNP-coated PA RO membrane were evaluated in a lab-scale cross-flow RO filtration system.

2. Materials and methods

2.1. Materials

Commercial PA RO membranes (RE-SHF) were kindly provided by the Toray Chemical Company (Korea). Titanium butoxide ($Ti(OC_4H_9)_4$, reagent grade, 97%), diethanolamine (DEA, $HN(C_2H_4OH)_2$, reagent grade, ≥98%), ammonium hydroxide (NH_4OH, 28% in H_2O), sodium chloride (anhydrous, ≥99.0%) and humic acid (technical grade) were purchased from Sigma-Aldrich. Ethanol (99.9%, Samchun Chemical, Korea) was chosen as the solvent for the TiO_2 sol-gel process.

2.2. Preparation of TiO_2 sol and TiO_2 nanoparticle–coated PA membrane

TiO_2 nanoparticles (TNPs) were synthesized by the base catalyzed TiO_2 sol-gel reaction. Ammonium hydroxide (100 μL), deionized water (DI water, 1 mL) and ethanol (16 mL) were mixed as the base catalyst and solvent, respectively. While maintaining vigorous stirring, titanium butoxide (2 mL) was injected into the ethanol, and the solution color changed to a white colored TiO_2 sol. After a 10 min stirring, 1 mL of 10 w/v% DEA/ethanol solution was injected into the TiO_2 sol as a stabilizer to slow down the hydrolysis and condensation reaction [22]. Finally, the TiO_2 sol was sonicated in a bath sonicator for 20 min. The prepared TiO_2 sol was deposited onto the PA membrane with the spray coating method. The PA RO membrane (10 cm × 10 cm) was fixed on a stainless plate, and a certain volume of TiO_2 sol was sprayed using an airbrush onto the PA RO membrane, and each membrane was designated as TNPROX. Note that TNPRO denotes the TiO_2 nanoparticles coated onto the PA RO membrane, and the X denotes the amount of the sprayed volume of TiO_2 sol on the PA RO membrane. After the sprayed solution evaporated, membrane samples were rinsed with DI water and stored in DI water before testing.

2.3. Surface characterization of the TNP-coated membranes

A field emission scanning electron microscope (FE-SEM; JSM-6701F, Jeol, Japan) was used to observe the surface morphology of the TNP coated and bare PA membranes. To obtain a clear SEM image, the membrane surface was coated with Pt by a sputter coater at 20 mA for 80 s. The electron composition of the TNP-coated membrane was analyzed using energy dispersive X-ray spectroscopy (EDS; JSM-6701F, Jeol, Japan). The surface hydrophilicity of the TNP coated and bare PA membranes were characterized with a sessile drop method by using a contact angle analyzer (DSA100, KRÜSS, Germany) [23]. The zeta potential of the TNP coated and bare PA membranes was analyzed with an electrophoretic light scattering spectrophotometer (ELS-8000, Otsuka Electronics, Japan). The TNPRO2.0 and bare PA membranes were analyzed by X-ray photoemission spectroscopy (XPS, Sigma Probe®, Thermo VG Scientific Co. Ltd., UK) specifically for carbon, oxygen, sulfur and titanium. Each element was scanned in 0.10 eV steps, and the element spectrum was fitted to the C1s peak (285.0 eV).

2.4. Permeate flux and salt rejection change

The permeate flux and salt rejection of the TNP-coated PA RO membranes were evaluated in a lab-scale cross-flow RO filtration system. More details about the system were described in our previous study [24]. In this study, 6 L of feed water containing 2,000 mg/L NaCl were used, and the effective membrane area was 22.4 cm^2 (3.3 cm × 6.8 cm) with a 0.3 cm channel height. The membrane performance test was performed with a cross-flow velocity of 8 cm s^{-1} at 25°C. After membrane compaction for 30 min. at 15.5 bar, the permeated water was collected in a bottle for 20 min. under the same pressure. The permeate flux and salt rejection were calculated according to Eqs. (1) and (2), respectively, as follows:

$$J_w = \frac{V}{A \times t} \tag{1}$$

$$R_s = \left[1 - \frac{C_p}{C_f}\right] \times 100 \tag{2}$$

where in Eq. (1), J_w is the permeate flux (LMH, L m^{-2} h^{-1}); V is the permeated volume of water; A is the effective membrane

area (m^2); t is the measuring time (h), and in Eq. (2), R_s is the NaCl rejection percentage ratio; C_f is the conductivity of the feed water (mS cm^{-1}), and C_p is the conductivity of the permeate (mS cm^{-1}). A conductivity meter (Horiba, Japan) was used to evaluate the salt rejection.

2.5. Organic fouling test of the TNP-coated membrane compared with the bare PA RO membrane

The organic fouling characteristics of the TNP coated and commercial PA RO membranes were evaluated by measuring the flux changes. The membranes were mounted in a membrane cell of the cross-flow RO filtration system. The operating conditions were as follows: an initial flux of 35 LMH and a cross-flow velocity of 4 cm s^{-1} at 25°C. The feed water consisted of 10 mM $CaCl_2$ and 1 mM NaCl. After the system was stabilized, 1,200 mg of humic acid were added to the feed water tank to adjust the humic acid concentration of the feed water to 200 mg L^{-1} of humic acid. The changes in the permeate flux were automatically recorded by computer every 30 min, and the fouling was carried out for 19 h.

An atomic force microscope (AFM, SPA-400, Seiko Instrument, Japan) was used to measure the interactive forces between the membrane surfaces and humic acid immobilized AFM tips (Nanosensors, CONTR, spring constant = 0.2 N m^{-1}). Similarly to our previous studies [25,26], the humic acid-immobilized AFM tips were prepared by a surface chemical reaction of an amine-terminated AFM tip and 100 mM humic acid solution. A speed of 0.1 mm s^{-1} was applied to obtain the force–extension curves during the approach and retraction of the membrane surfaces from the humic acid-immobilized AFM tip. All experiments were carried out in water at room temperature. Approximately 50 approach/retract cycles were performed for each membrane surface collected.

3. Results and discussion

3.1. Characterization of the TNP membranes

Fig. 1 shows the SEM images of the TNP coated and bare PA RO membranes. As shown in Fig. 1(a), the size of the TNPs, which were deposited on the TNPRO2.0 with the sol-gel derived spray coating method, appeared to be 30–50 nm. In Figs. 1(b)–(e), the TNP-coated membranes show that the ridge and alley structure of the bare PA membrane (Fig. 1(f)) surface was covered with TNPs, and the TNP-coated area increased with the amount of sprayed TiO_2 sol.

The TNP coating layer on the PA RO membrane was also examined by EDS analysis (Fig. 2). Fig. 2(a) shows the titanium weight concentration change of the TNP-coated membranes as a function of the TNP coating amount on the PA RO membrane. The titanium weight concentration of the TNP-coated membranes gradually increased from 1.2% to 5.1% as the increased coating amount of the TiO_2 sol while the commercial PA RO membrane showed no titanium. EDS mapping analysis also revealed that the observed coating layer consists of TiO_2. Figs. 2(c)–(e) show the carbon, titanium and oxygen elemental mapping of the TNPRO2.0. Note that the red, green and yellow colors indicate carbon, titanium and oxygen, respectively, and the brightness difference of the color implies the amount of each element. While the carbon signal (Fig. 2(c)) was detected uniformly with no difference in brightness and in titanium and oxygen signals (Figs. 2(d) and (e)) showed various intensities for the signals, and its morphology was very similar with the coating layer on the TNPRO2.0 observed by SEM image (Fig. 2(b)).

Fig. 3 shows the XPS spectrum of the TNPRO2.0 compared with the bare PA RO membrane. As shown in Fig. 3, two main changes were observed in the XPS spectrum. First, a Ti and Ti–O peak was detected in the TNPRO2.0 after the TNP coating. The titanium spectrum of the TNP2.0 had four

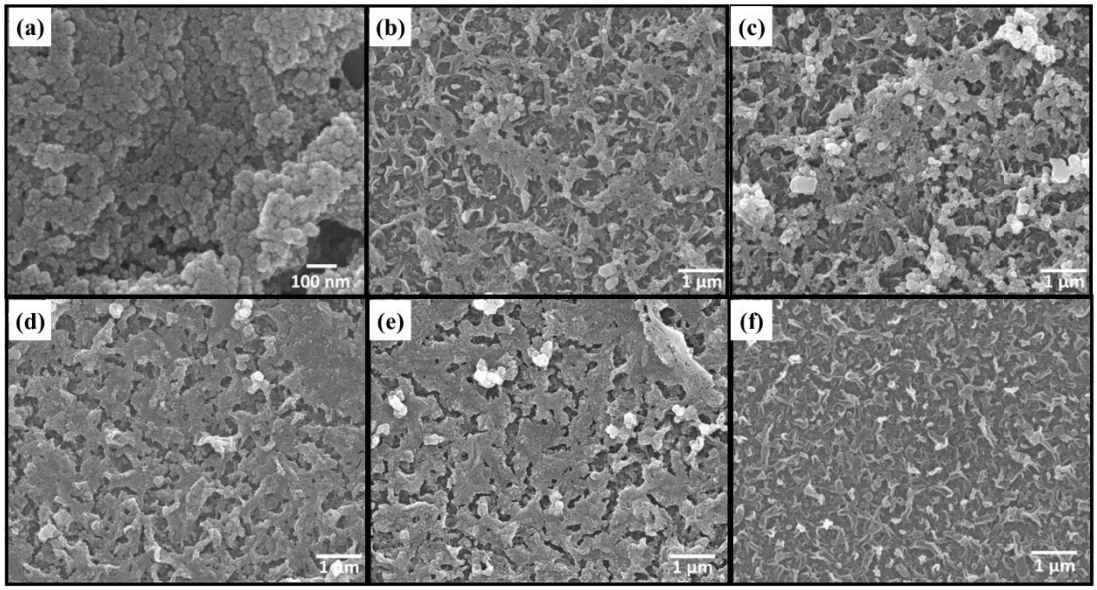

Fig. 1. SEM images of (a) TiO_2 nanoparticles on the PA membrane (enlarged image of TNPRO2.0), (b) TNPRO0.5, (c) TNPRO1.0, (d) TNPRO1.5, (e) TNPRO2.0 and (f) bare PA (Note that TNPRO denotes the TiO_2 nanoparticle–coated membrane and the number denotes the amount of sprayed TiO_2 sol on the PA RO membrane).

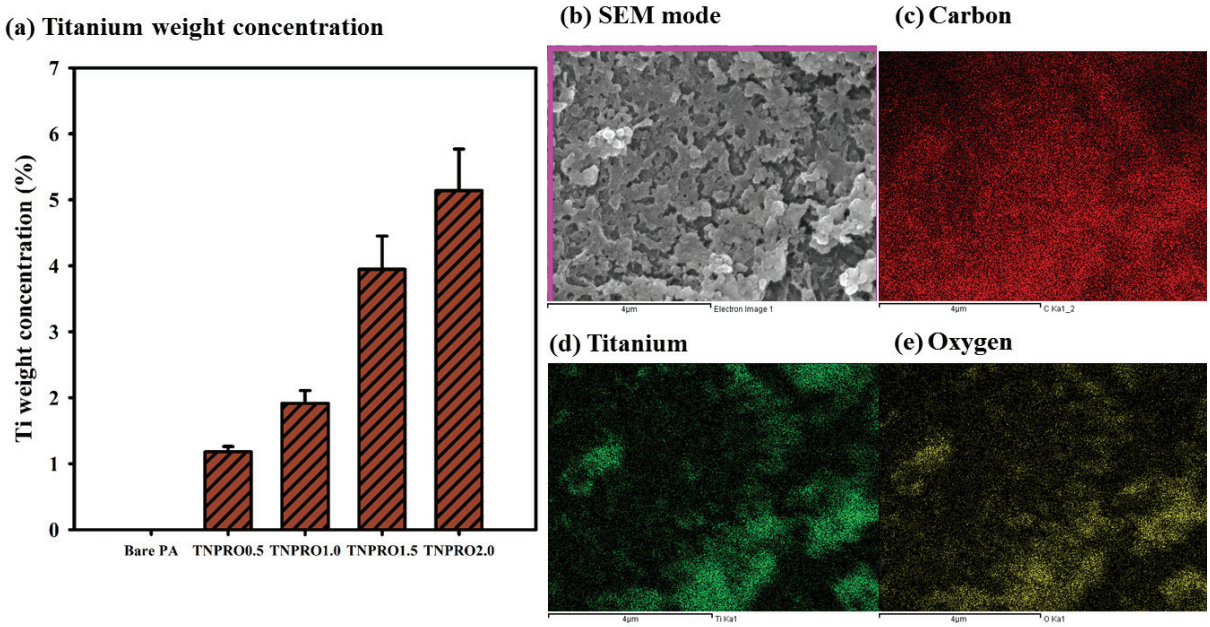

Fig. 2. EDS analysis results: (a) titanium weight concentration of the TNP membranes, (b) SEM image of the TNPRO2.0 membrane and its elemental mapping of (c) carbon, (d) titanium and (e) oxygen (Note that TNPRO denotes the TiO_2 nanoparticle–coated membrane and the number denotes the amount of sprayed TiO_2 sol on the PA RO membrane).

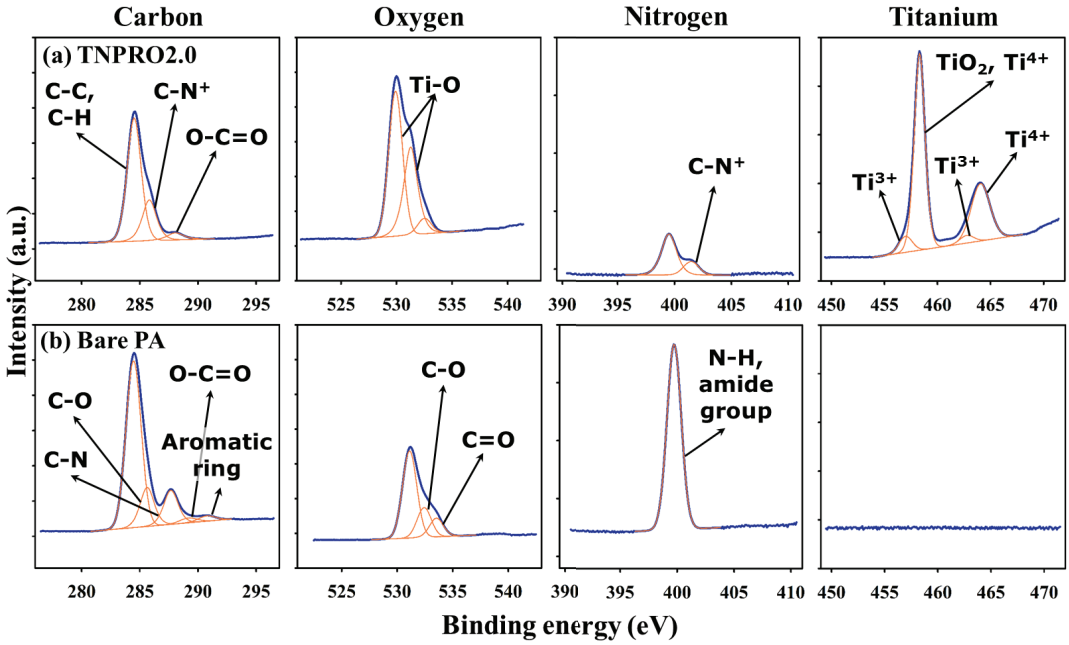

Fig. 3. Comparison of the X-ray photoelectron spectroscopy spectrum for (a) TNPRO2.0 and (b) bare PA membrane in terms of the carbon, oxygen, nitrogen and titanium (Note that TNPRO denotes the TiO_2 nanoparticle–coated membrane, and the number denotes the amount of sprayed TiO_2 sol on the PA RO membrane).

titanium peaks as follows: Ti 2p3/2 (457–459 eV), Ti 2p1/2 (463–464 eV), Ti^{3+} (457.0 and 462.8 eV), and Ti^{4+} (458.3 and 464.1 eV) [27,28]. In the oxygen spectrum, Ti–O peaks at 529.9 and 531.3 eV were found after the TNP coating [29,30]. These formations of the Ti and Ti–O peaks obviously indicate that TiO_2 was synthesized from titanium butoxide by the base catalyzed sol-gel method. To confirm this result, attenuated total reflectance Fourier transform infrared (ATR-FTIR) analysis was performed (data not shown). In the range of 450–700 cm^{-1}, several peaks, which might be attributed to

the Ti–O–Ti bond, were detected, and this also supports the formation of TiO_2 [31,32]. On the other hand, the TiO_2 layer coated on the PA surface blocks the XPS signal from the PA layer or weakens the peak intensity of PA layer. The C–O peaks (285.6 eV), C–N peak (287.7 eV), C=O peak (533.5 eV) and aromatic ring peak (290.9 eV) disappeared, and the peak intensities of C–C (284.5 eV), C–O (532.4 eV) and C–N (399.7 eV) were reduced after the TiO_2 coating [33–36]. It seems that the deposition of the TiO_2 coating layer reduces or hides the XPS signal of the PA layer due to the low XPS penetration depth. The peaks at 285.8 and 401.5 eV corresponding to the $C–N^+$ bond were generated in the TNPRO2.0 [36,37]. This might be the reason that the basic TiO_2 sol leads to the release of protons from the amide group of the PA layer.

Table 1 presents the contact angle and zeta potential of the TNP-coated membranes. The average contact angle of the TNP membranes gradually decreased from 23.6° to 5.8° as the coating amount of the TNP was increased while that of the bare PA was 43.6°. This result apparently indicates that the TNP coating formed a more hydrophilic surface on the TNP membrane. The zeta potentials of TNPRO0.5, TNPRO1.0, TNPRO1.5 and TNPRO2.0 were –25, –29.8, –30.9 and –40.1 mV, respectively. The TNP-coated membranes showed a greatly increased negative charge compared with the bare PA (–10.6 mV), and as the TiO_2 coating amount was increased, the surface zeta potential gradually decreased. This result is consistent with previous studies showing that the surface charge of TiO_2 is negative in a neutral or base condition [38–40]. Therefore, it could be interpreted that the surface coating of the TNP changed the charge of the PA RO membrane surface to negative due to the negative charge of the TiO_2.

Fig. 4 shows the effect of the TNP coating on the permeate flux and salt rejection of the PA membrane. In our cross-flow RO membrane system, the permeate flux and salt rejection of the bare PA membrane was 27.6 LMH (blue dashed line) and 98.2% (gray dotted line), respectively. As shown in Fig. 4, while up to 2.0 mL of the TNP coating on the membrane showed only a negligible difference in the membrane performance (i.e., the permeate flux and salt rejection) compared with the bare PA membrane, TNPRO4.0 exhibited a decreased performance. This result could be explained by external concentration polarization caused by the deposited TNP on the PA membrane [7,41,42]. It seems that the large amount of TNPs on the TNPRO4.0 caused the accumulation

Table 1
Sessile drop contact angle and surface zeta potential of the TNP-coated membranes compared with the bare PA membrane (Note that TNPRO denotes the TiO_2 nanoparticle–coated membrane, and the number denotes the amount of sprayed TiO_2 sol on the PA RO membrane)

Membrane	Contact angle (°)	Zeta potential (mV)
TNPRO0.5	23.6 ± 0.9	–25.0 ± 1.6
TNPRO1.0	16.3 ± 2.7	–29.8 ± 1.2
TNPRO1.5	7.8 ± 2.4	–30.9 ± 0.9
TNPRO2.0	5.8 ± 2.2	–40.1 ± 0.4
Bare PA	43.6 ± 1.2	–10.6 ± 0.2

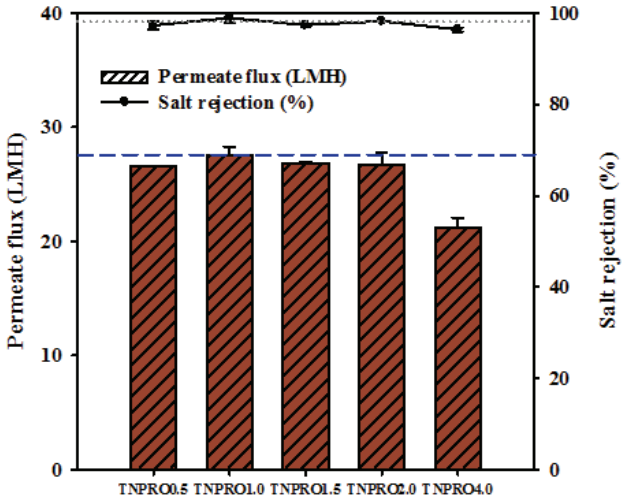

Fig. 4. Permeate flux and salt rejection change of the TNP-coated membranes as a function of the TNP coating amount on the PA membrane (gray dotted line: salt rejection of the bare PA; blue dashed line: permeate flux of the bare PA; the test was carried out in the cross-flow filtration system; cross-flow velocity and temperature: 8 cm s^{-1} and 25°C; feed water: 2,000 mg/L NaCl; Note that TNPRO denotes the TiO_2 nanoparticle–coated membrane and the number denotes the amount of sprayed TiO_2 sol on the PA RO membrane).

of salt on the membrane surface and increased the osmotic pressure, consequently, decreasing the permeate flux and salt rejection rate, whereas the appropriate coating amount of TNPRO2.0 maintained the performance of the membrane.

The anti-fouling performance of TNPRO2.0 compared with the bare PA was evaluated under humic acid filtration condition and is shown in Fig. 5(a). As seen in Fig. 5(a), TNPRO2.0 showed only a 6% flux decline for 5 h, while the bare PA showed a 28% reduced flux. The normalized flux gap between the TNPRO2.0 and the bare PA was 26% at the end of the experiment (19 h). Because the accumulation of humic acid causes a permeate flux decline, Fig. 5(a) shows that a smaller quantity of humic acid was deposited on the TNPRO2.0 compared with the bare PA membrane. It is reported that a hydrophobic and less negatively charged membrane is easily fouled with humic acid due to the negative and hydrophobic surface property of the humic acid [43]. As presented in Table 1, the surface property of the membrane became more hydrophilic and more negatively charged, which consequently reduced the foulant–membrane interaction [9]. The interactive forces between the humic acid–tethered AFM tip and membrane surface of the TNPRO2.0 and the bare PA membranes clearly show this correlation (Fig. 5(b)). As shown in Fig. 5(b), during retraction, no interactive force (red circle) was found on the TNPRO2.0, while the bare PA showed a 0.15 nN pull-off force (black arrow). This result implies that the TNP coating on the PA membrane reduced the attractive force to humic acid. Therefore, the enhanced membrane surface property could be attributed to fouling resistance against humic acid. This result is consistent with a previous study [12]. The surface modified RO membrane by grafting PEG exhibited a fouling resistance due to the increased hydrophilicity and negative charge.

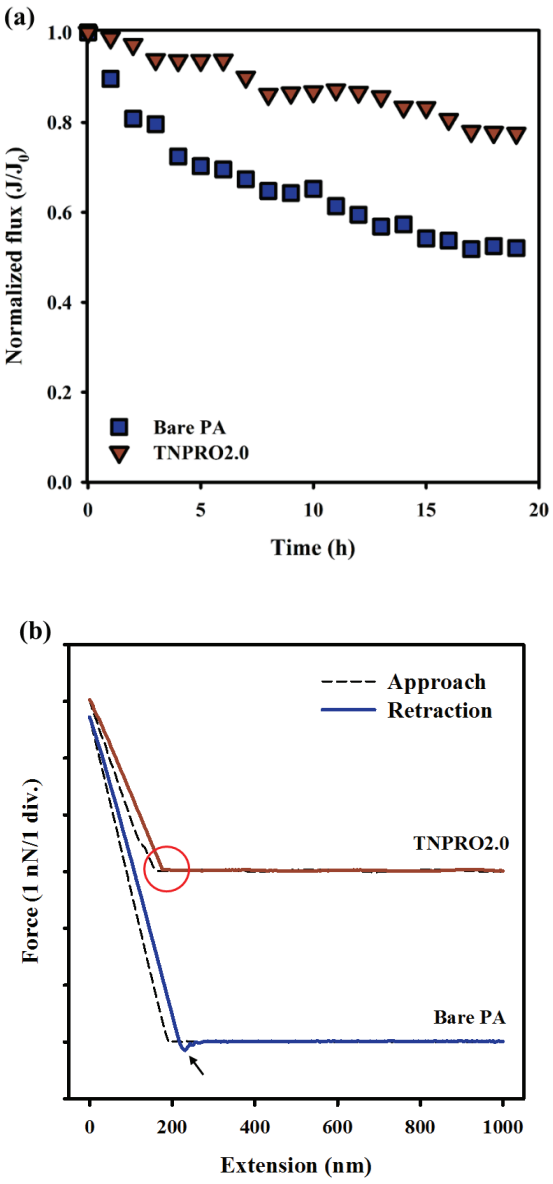

Fig. 5. Organic fouling property of the TNPRO2.0 membrane compared with the bare PA membrane (a) normalized flux change under humic acid filtration condition (Initial permeate flux: 35 LMH; feed water: 10 mM NaCl, 1 mM $CaCl_2$ and 200 mg/L humic acid; cross-flow velocity and temperature: 4 cm s^{-1} and 25°C; time "0" means the dosing point of humic acid into the feed water; Note that TNPRO denotes the TiO_2 nanoparticle–coated membrane, and the number denotes the amount of sprayed TiO_2 sol on the PA RO membrane) (b) interactive force between the humic acid tethered AFM tip and the membrane surface.

4. Conclusion

In this study, we propose a facile surface modification to fabricate a fouling resistant PA RO membrane with the TiO_2 sol-gel derived spray coating method. A TiO_2 nanoparticle solution was made by the base catalyzed sol-gel method. The results of SEM, EDS and XPS confirmed that the surface of the PA RO membrane was successfully coated with TNPs. The TNP-coated PA RO membrane maintained its permeate flux and salt rejection when 2.0 mL of TiO_2 sol was coated onto the membrane surface and exhibited an increased hydrophilicity and negatively charged surface property. These surface changes reduced the interactive force between humic acid and the membrane surfaces, consequently, resulting in a 26% less flux reduction than that of the bare PA RO membrane during 19 h of humic acid fouling.

Acknowledgments

This research was supported by grant (code 17IFIP-B088091-04) from Industrial Facilities & Infrastructure Research Program and funded by Ministry of Land, Infrastructure and Transport of Korean government, and by Korea Ministry of Environment as "Global Top Project (E617-00211-0608-0)."

References

[1] M. Elimelech, W.A. Phillip, The future of seawater desalination: energy, technology, and the environment, Science, 333 (2011) 712–717.
[2] V.S. Frenkel, Seawater Desalination: Trends and Technologies, INTECH Open Access Publisher, 2011.
[3] L.F. Greenlee, D.F. Lawler, B.D. Freeman, B. Marrot, P. Moulin, Reverse osmosis desalination: water sources, technology, and today's challenges, Water Res., 43 (2009) 2317–2348.
[4] J. Wu, Z. Wang, W. Yan, Y. Wang, J. Wang, S. Wang, Improving the hydrophilicity and fouling resistance of RO membranes by surface immobilization of PVP based on a metal-polyphenol precursor layer, J. Membr. Sci., 496 (2015) 58–69.
[5] D. Potts, R. Ahlert, S. Wang, A critical review of fouling of reverse osmosis membranes, Desalination, 36 (1981) 235–264.
[6] X. Zhu, M. Elimelech, Colloidal fouling of reverse osmosis membranes: measurements and fouling mechanisms, Environ. Sci. Technol., 31 (1997) 3654–3662.
[7] E.M. Hoek, M. Elimelech, Cake-enhanced concentration polarization: a new fouling mechanism for salt-rejecting membranes, Environ. Sci. Technol., 37 (2003) 5581–5588.
[8] G.D. Kang, Y.M. Cao, Development of antifouling reverse osmosis membranes for water treatment: a review, Water Res., 46 (2012) 584–600.
[9] D. Rana, T. Matsuura, Surface modifications for antifouling membranes, Chem. Rev., 110 (2010) 2448–2471.
[10] L. Zou, I. Vidalis, D. Steel, A. Michelmore, S.P. Low, J.Q.J.C. Verberk, Surface hydrophilic modification of RO membranes by plasma polymerization for low organic fouling, J. Membr. Sci., 369 (2011) 420–428.
[11] J. Gilron, S. Belfer, P. Väisänen, M. Nyström, Effects of surface modification on antifouling and performance properties of reverse osmosis membranes, Desalination, 140 (2001) 167–179.
[12] G. Kang, M. Liu, B. Lin, Y. Cao, Q. Yuan, A novel method of surface modification on thin-film composite reverse osmosis membrane by grafting poly(ethylene glycol), Polymer, 48 (2007) 1165–1170.
[13] A.C. Sagle, E.M. Van Wagner, H. Ju, B.D. McCloskey, B.D. Freeman, M.M. Sharma, PEG-coated reverse osmosis membranes: desalination properties and fouling resistance, J. Membr. Sci., 340 (2009) 92–108.
[14] R. Yang, J. Xu, G. Ozaydin-Ince, S.Y. Wong, K.K. Gleason, Surface-tethered zwitterionic ultrathin antifouling coatings on reverse osmosis membranes by initiated chemical vapor deposition, Chem. Mater., 23 (2011) 1263–1272.
[15] C. Kim, S. Kim, J. Lee, J. Kim, J. Yoon, Capacitive and oxidant generating properties of black-colored TiO_2 nanotube array fabricated by electrochemical self-doping, ACS Appl. Mater. Interfaces, 7 (2015) 7486–7491.

[16] S.-Y. Kwak, S.H. Kim, S.S. Kim, Hybrid organic/inorganic reverse osmosis (RO) membrane for bactericidal anti-fouling. 1. Preparation and characterization of TiO_2 nanoparticle self-assembled aromatic polyamide thin-film-composite (TFC) membrane, Environ. Sci. Technol., 35 (2001) 2388–2394.
[17] S.H. Kim, S.-Y. Kwak, B.-H. Sohn, T.H. Park, Design of TiO_2 nanoparticle self-assembled aromatic polyamide thin-film-composite (TFC) membrane as an approach to solve biofouling problem, J. Membr. Sci., 211 (2003) 157–165.
[18] S.S. Madaeni, N. Ghaemi, Characterization of self-cleaning RO membranes coated with TiO_2 particles under UV irradiation, J. Membr. Sci., 303 (2007) 221–233.
[19] Y. Takahashi, Y. Wada, Dip-coating of Sb-doped SnO_2 films by ethanolamine-alkoxide method, J. Electrochem. Soc., 137 (1990) 267–272.
[20] D.J. Kim, S.H. Hahn, S.H. Oh, E.J. Kim, Influence of calcination temperature on structural and optical properties of TiO_2 thin films prepared by sol–gel dip coating, Mater. Lett., 57 (2002) 355–360.
[21] R.S. Sonawane, B.B. Kale, M.K. Dongare, Preparation and photo-catalytic activity of Fe–TiO_2 thin films prepared by sol–gel dip coating, Mater. Chem. Phys., 85 (2004) 52–57.
[22] S. Kahraman, S. Çetinkaya, H.A. Çetinkara, H.S. Güder, Effects of diethanolamine on sol–gel–processed Cu_2ZnSnS_4 photovoltaic absorber thin films, Mater. Res. Bull., 50 (2014) 165–171.
[23] C. Kim, J. Lee, S. Kim, J. Yoon, TiO_2 sol–gel spray method for carbon electrode fabrication to enhance desalination efficiency of capacitive deionization, Desalination, 342 (2014) 70–74.
[24] Y. Baek, J. Yu, S.-H. Kim, S. Lee, J. Yoon, Effect of surface properties of reverse osmosis membranes on biofouling occurrence under filtration conditions, J. Membr. Sci., 382 (2011) 91–99.
[25] H.J. Kim, D.-G. Kim, H. Yoon, Y.-S. Choi, J. Yoon, J.-C. Lee, Polyphenol/FeIII complex coated membranes having multifunctional properties prepared by a one-step fast assembly, Adv. Mater. Interfaces, 2 (2015) 1500298.
[26] D.-G. Kim, H. Kang, S. Han, J.-C. Lee, The increase of antifouling properties of ultrafiltration membrane coated by star-shaped polymers, J. Mater. Chem., 22 (2012) 8654–8661.
[27] J.D. Grunwaldt, U. Göbel, A. Baiker, Preparation and characterization of thin TiO_2-films on gold/mica, Fresenius' J. Anal. Chem., 358 (1997) 96–100.
[28] C. Chen, H. Bai, C. Chang, Effect of plasma processing gas composition on the nitrogen-doping status and visible light photocatalysis of TiO_2, J. Phys. Chem. C, 111 (2007) 15228–15235.
[29] M.Z. Atashbar, H.T. Sun, B. Gong, W. Wlodarski, R. Lamb, XPS study of Nb-doped oxygen sensing TiO_2 thin films prepared by sol-gel method, Thin Solid Films, 326 (1998) 238–244.
[30] P.Y. Jouan, M.C. Peignon, C. Cardinaud, G. Lempérière, Characterisation of TiN coatings and of the TiN/Si interface by X-ray photoelectron spectroscopy and Auger electron spectroscopy, Appl. Surf. Sci., 68 (1993) 595–603.
[31] W. Zhang, J. Shi, X. Wang, Z. Jiang, X. Song, Q. Ai, Conferring an adhesion layer with mineralization-inducing capabilities for preparing organic–inorganic hybrid microcapsules, J. Mater. Chem. B, 2 (2014) 1371–1378.
[32] N. Nakayama, T. Hayashi, Preparation and characterization of poly(l-lactic acid)/TiO_2 nanoparticle nanocomposite films with high transparency and efficient photodegradability, Polym. Degrad. Stab., 92 (2007) 1255–1264.
[33] K. Yamamoto, Y. Koga, S. Fujiwara, XPS studies of amorphous SiCN thin films prepared by nitrogen ion-assisted pulsed-laser deposition of SiC target, Diamond Relat. Mater., 10 (2001) 1921–1926.
[34] L. Matuana, J. Balatinecz, R. Sodhi, C. Park, Surface characterization of esterified cellulosic fibers by XPS and FTIR spectroscopy, Wood Sci. Technol., 35 (2001) 191–201.
[35] S. Delpeux, F. Beguin, R. Benoit, R. Erre, N. Manolova, I. Rashkov, Fullerene core star-like polymers—1. Preparation from fullerenes and monoazidopolyethers, Eur. Polym. J., 34 (1998) 905–915.
[36] J. Charlier, V. Detalle, F. Valin, C. Bureau, G. Lecayon, Study of ultrathin polyamide-6, 6 films on clean copper and platinum, J. Vacuum Sci. Technol. A, 15 (1997) 353–364.
[37] V. Wiertz, P. Bertrand, Identification of the N-containing functionalities introduced at the surface of ammonia plasma treated carbon fibres by combined ToF-SIMS and XPS, 1998.
[38] G. Parfitt, The surface of titanium dioxide, Prog. Surf. Membr. Sci, 11 (1976) 181–226.
[39] T. Hanawa, M. Kon, H. Doi, H. Ukai, K. Murakami, H. Hamanaka, K. Asaoka, Amount of hydroxyl radical on calcium-ion-implanted titanium and point of zero charge of constituent oxide of the surface-modified layer, J. Mater. Sci. Mater. Med., 9 (1998) 89–92.
[40] K. Suttiponparnit, J. Jiang, M. Sahu, S. Suvachittanont, T. Charinpanitkul, P. Biswas, Role of surface area, primary particle size, and crystal phase on titanium dioxide nanoparticle dispersion properties, Nanoscale Res. Lett., 6 (2011) 1–8.
[41] S. Sablani, M. Goosen, R. Al-Belushi, M. Wilf, Concentration polarization in ultrafiltration and reverse osmosis: a critical review, Desalination, 141 (2001) 269–289.
[42] E. Matthiasson, B. Sivik, Concentration polarization and fouling, Desalination, 35 (1980) 59–103.
[43] J. Cho, G. Amy, J. Pellegrino, Membrane filtration of natural organic matter: comparison of flux decline, NOM rejection, and foulants during filtration with three UF membranes, Desalination, 127 (2000) 283–298.